CrystEngComm

Accepted Manuscript

ROYAL SOCIETY OF CHEMISTRY

www.rsc.org/crystengcomm

Cite this: DOI: 10.1039/c0xx00000x

www.rsc.org/xxxxxx

ARTICLE TYPE

Effects of Sn atoms on formation of ZnO nanoring

Ramin Yousefi

Received (in XXX, XXX) Xth XXXXXXXXX 20XX, Accepted Xth XXXXXXXXX 20XX
DOI: 10.1039/b000000x

Sn-doped ZnO nanobelts (NBs) and nanorings were grown on Si(100) substrates with the assistance of a gold catalyst, using a thermal evaporation method. The source material was placed at 1100 °C, while the substrates were placed at 700 and 800 °C. ZnO NBs with different sizes were obtained at the different substrate temperatures. In addition, undoped ZnO NBs were grown under the same conditions. Field emission scanning electron microscope (FESEM) images showed that some nanorings were formed at the ends of the Sn-doped ZnO NBs, whereas no nanorings were observed for the undoped ZnO NBs. Furthermore, these images showed that some NBs were grown via a vapor–liquid–solid (VLS) mechanism. High-magnification transmission electron microscope (HRTEM) images and the selected area electron diffraction (SAED) pattern showed that the Sn-doped ZnO NBs were grown along the [01$\bar{1}$0] direction. In addition, a HRTEM image of a single Sn-doped ZnO NB revealed that the nanorings were formed as a result of planar defects. The X-ray diffraction (XRD) patterns indicated a wurtzite phase for the undoped and doped ZnO NBs. Room temperature photoluminescence (PL) spectroscopy and the UV–vis diffuse reflectance spectra (DRS) measurements were used to study optical properties of the nanostructures. The PL and DRS results showed that, the band gap of Sn-doped ZnO NBs were widened in comparison to the band gap of undoped ZnO NBs. Finally, the samples were characterized by X-ray photoelectron spectroscopy (XPS) and it was observed a relationship between the XPS results and O vacancy of the ZnO NBs.

Introduction

From a nanoscience and nanotechnology point of view, it is useful to study the different morphologies of materials such as ZnO, which has several applications such as photocatalysts, optoelectronics, lasing, gas sensing, and piezoelectricity. In addition tunable properties of doped ZnO nanostructures cause to obtain interesting applications for ZnO nanostructures.[1-2] The important characteristics of a wurtzite structure such as ZnO are the noncentral symmetry and polar surfaces. The structure of ZnO can be described as a number of alternating planes composed of tetrahedrally coordinated O^{2-} and Zn^{2+} ions, stacked alternately along the *c* axis. The oppositely charged ions produce positively charged (0001)-Zn and negatively charged (0001)-O polar surfaces, resulting in a normal dipole moment and spontaneous polarization along the *c* axis, as well as a divergence in surface energy.[3] According to detailed microscopic study, a structure such as ZnO can be grown via three types of fast growth directions: <2$\bar{1}\bar{1}$0> (±[2$\bar{1}\bar{1}$0], ±[$\bar{1}$2$\bar{1}$0], ±[$\bar{1}\bar{1}$20]); <01$\bar{1}$0> (±[01$\bar{1}$0], ±[10$\bar{1}$0], ±[1$\bar{1}$00]); and ±[0001]. Together with the polar surfaces due to atomic terminations, ZnO exhibits a wide range of novel structures that can be grown by tuning the growth rates along these directions.[4] Some of the most important factors to obtain different structures and morphologies are the growth conditions. A minor variation in the growth conditions may result in a great change in the morphology and structure of the final product. One-dimensional (1-D) ZnO nanostructures are usually grown with wire and belt morphologies with low index crystallographic faces. These structures tend to maximize the areas of the {2$\bar{1}\bar{1}$0} and {01$\bar{1}$0} facets because of the lower energy.[4]

The belt-like nanostructure morphology is a common structural characteristic for functional oxides with different crystallographic structures. In fact, ZnO nanobelts (NBs) can be grown with three structures.[5] One of these structures can be grown by introducing planar defects. ZnO NBs have several applications. Addition of ZnO NBs, ZnO nanorings are interesting morphology of ZnO that can be formed via ZnO NBs.[6] According to a microscopic study, planar defects are essential for the formation of nanorings.[3] Planar defects can be twins, conventional stacking faults, or interstitial stacking layers introduced by impurity atoms.[7] Wang's group could form ZnO nanorings using indium as the dopant element.[5] They also showed that planar defects as inversion domain boundaries (IDBs) could be introduced into ZnO NBs by indium ion doping. They observed that the head-to-head and tail-to-tail paired IDBs did not change the polarity of the NB. Therefore, a nanoring was initiated by circularly folding a NB because of the long-range electrostatic interaction between the surface polar charges on the two sides, and a loop-by-loop winding of the NB formed a complete ring. They used *In* as the doping material because indium doping is important in the semiconductor industry, and many research groups in addition to ours have focused on the development of In-doped ZnO nanostructures in recent years.[8-11] In addition to indium, tin (Sn) is an important doping material that can introduce new applications for ZnO.[12-19] It is known that the band-gap of ZnO can be fine tuned by alloying ZnO with another material with a different band-gap, thus affecting the wavelength

of the exciton emission. Thus, the alloying of ZnO with SnO_2 creates a ZnO/SnO_2 structure, as a potential candidate for future optoelectronic devices, because the addition of SnO_2, which has a larger band-gap (3.6–3.97 eV) than ZnO, results in a widened band-gap. In addition, Sn-doped ZnO nanowires exhibit significantly improved field emission characteristics in comparison with undoped ones and reduced resistance as the Sn content increases.[20] In addition to the effects of Sn on the optical band gap and improved electrical properties, Sn can play a role as a doping material that causes the formation of planar defects in ZnO NBs.[21] Therefore, ZnO nanorings can be formed using Sn as a dopant material, which has not previously been reported. However, the effects of the Sn concentration on the formation of ZnO nanorings have not yet been studied. In addition, the vapor–liquid–solid (VLS) method, which is one of the most important methods for growing 1-D nanostructures, has not yet been applied to grow ZnO nanorings.

For these reasons, in this work, a sintering method was used to prepare a ZnO/SnO_2 compound as the source material. Using this material, Sn-doped ZnO NBs and nanorings were grown on Si(100) substrates that were placed in different temperature zones using gold metal as the catalyst in the presence of a mixture of argon and oxygen as a carrier gas in a conventional tube furnace. This paper shows that the use of Sn as an impurity can form planar defects in ZnO NB structures, which results in the formation of ZnO nanorings.

Experimental

The ZnO nanostructures were deposited in a conventional horizontal furnace. First, Si(100) substrates were ultrasonically cleaned using ethanol and de-ionized water, and then, they were lightly etched using HF (43%) mixed with de-ionized water (1:10) for about 10 min to remove the native oxide layer. A gold layer with a thickness of about 20 nm, serving as a metal catalyst, was deposited on the substrates using a sputtering technique. Zinc oxide (99.99%) and tin dioxide powders (99.99%) were mixed at a weight ratio of 10:1 and then pressed into a small pill under a pressure of 40 MPa. This pill was calcined in a box furnace at 500 °C for 5 h and sintered at 900 °C for 12 h in air, thereby producing a pill of the ZnO/SnO_2 compound. After the heat treatment, the pill was ground into powder again. Then, the powder was placed on an alumina boat and inserted into a horizontal tube furnace, in order to serve as the evaporation source. Silicon substrates were located downstream from the source material. The source material was heated to 1100 °C, and the temperature of the substrates was maintained between 700 and 800 °C during the growth process. A mixture of high purity Ar/O_2 (10:1) gas was fed at about 100 sccm into the tube furnace at one end, while the other end was connected to a rotary pump. The growth process was allowed to proceed for 1 h. A vacuum of 10 Torr was maintained inside the tube furnace during the deposition of the nanostructures.

The crystal structure and morphology of the products were investigated by field emission scanning electron microscopy (FESEM, Quanta 200F) and X-ray diffraction (XRD, Siemens D5000). Elemental analyses of the products were conducted using an energy-dispersive X-ray spectroscope (EDX), which was attached to a field emission scanning electron microscope (FESEM, Quanta 200 F), field emission Auger electron spectroscopy (AES, JAMP-9500F), and using X-ray photoelectron spectroscopy (XPS; VG-Microtech ESCA-2000). The XPS spectra were recorded using Mg-K_α radiation (1256.6 eV). The room temperature photoluminescence (PL, Jobin Yvon Horiba HR 800 UV) by He-Cd laser with a wavelength of 325nm as the excitation source at a 20mW power level and the UV–vis diffuse reflectance spectra (DRS) with a UV–visible spectrophotometer (JASCO, UV-670) over a wavelength range of 200–800 nm were employed to study of the optical properties of ZnO nanostructures.

Results and discussion

Figure 1(a–f) shows FESEM images of the undoped (Fig. 1(f)) and Sn-doped ZnO NBs (Fig. 1(a–e)) deposited at the different substrate temperatures. Figure 1(a–b) shows low and high magnification images of the Sn-doped ZnO NBs grown on substrates that were placed at 700 °C. In addition, the EDX spectrum of this sample is shown in Fig. 1(a). The EDX spectrum indicates the presence of Sn in this sample. The inset of Fig. 1(b) shows a single NB that has a gold particle on its tip. The Au caps on the tips of the NBs confirm that the ZnO NBs were grown using the VLS method. A more careful examination of the image shows that this sample includes some dual nanorings (Fig. 1(c)). These nanorings started to grow from a single point of the NB. Figure 1(d–e) shows low and high magnification images of Sn-doped ZnO NBs that were grown on substrates that were placed at 800 °C. The EDX spectrum of these NBs also indicates the presence of Sn in this sample. However, a comparison between two EDX spectra results shows that the Sn concentration was greater in the sample that was placed at 700 °C compared to the sample that was placed at 800 °C. In addition, the inset of Fig. 1(e) shows a gold particle on the tip of a single NB. Therefore, the NBs in this sample were also grown using the VLS method. Furthermore, FESEM images of this sample reveal that the width of the NBs in this sample is smaller than the width of the NBs that were grown on a cooler substrate. It is known that the substrate temperature is the most important factor to obtain nanostructures with different sizes.[22] In fact, the size of the nucleating nanocrystals, which form at certain locations to relieve strain, increases with decreasing substrate temperature. At high substrate temperatures, rapid NB growth begins immediately after nanocrystal formation, freezing in the minimum nanocrystal diameter. For decreasing substrate temperature, the nanocrystals have a greater opportunity to grow laterally in order to distribute the strain relief. Figure 1(e) shows that the Sn-doped ZnO NBs that were grown at 800 °C also included nanorings. In addition to Sn-doped ZnO NBs, undoped ZnO NBs were also grown under the same conditions with and without the gold assistant. Figure 1(f) shows undoped ZnO NBs that were grown at 700 °C without gold. We did not observe any nanorings in the undoped samples. In fact, we wanted to determine whether or not a gold catalyst causes the formation of nanorings. In addition, we examined the growth conditions for Sn-doped ZnO without gold. The nanorings

were formed again without gold. However, we could not find any dual nanoring in the sample that was grown without the gold catalyst. In fact, it was understood that the Sn ion was the most important factor to obtain nanorings, and gold was the most important factor to obtain dual nanorings. However, our further studies will confirm these claims. The EDX spectra of different points of the dual-nanoring (not shown here) show that the tip point of the NB that was connected to the dual-nanoring had Zn, O, Sn, and Au elements. In fact, this result proved that the NB connected to the dual-nanoring was grown using the VLS method. On the other hand, the EDX results from the other points of the dual-nanoring show only Zn, O, and Sn peaks.

Figure 2(a) and (b) shows low and high magnification TEM images of Sn-doped ZnO NBs that were grown at 700 °C. It can be seen that the NBs have the same width (around 80 nm) with a length of several micrometers. In addition, Fig. 2(b) clearly shows the gold particle that was formed at the end of a single NB. Figure 2(c) and (d) reveals a SAED pattern and HRTEM image of the Sn-doped ZnO NB. The SAED pattern shows that the NB is single crystalline and indicates that the phase of the NB is of the wurtzite ZnO structure. According to the SAED pattern and HRTEM image, it can be understood that the NB was grown along the $[01\bar{1}0]$ direction. In addition, arrows show the planar defects in the HRTEM image of the NBs shown in Fig. 2(d). Therefore, the nanorings obtained here were formed as a result of planar defects that were formed as a result of the Sn doping. This method caused the direction of the NB growth to become $[01\bar{1}0]$, with side surfaces $\pm(2\bar{1}\bar{1}0)$. In fact, the polar-charge induced formation of the nanoring was driven by minimizing energy. Thereby, the self-coiling of the dual-nanoring was likely to be driven by minimizing the energy contributed by the polar charges, surface area, and elastic deformation.[23] The mechanism of the ZnO dual nanoring formation is shown schematically in Fig. 3. In this figure, the planar defects are parallel to the $<01\bar{1}0>$ direction. Based on the obtained results, a growth mechanism for the dual-nanorings can be tentatively proposed. Kong and Wang proposed a relationship between the ring diameter and belt thickness using the following equation: [23]

$$(t/R)^{*}=24\sigma^{2}/\varepsilon\varepsilon_{0}Y \quad (1)$$

where t, R, σ, ε, and Y are the thickness, radius, surface charge density, dielectric constant, and bending modulus of the NB, respectively. It can be seen that the radius of a nanoring is directly dependent on the thickness of the NB. Based on this equation, the possibility can be proposed that at the end of the NBs that were connected to the dual-nanorings, the gold droplet split into two branches with different thickness. In fact, this phenomenon occurs sometimes if the gold droplet is not stable during growth.[24] In fact, this phenomenon causes two NBs with different thicknesses to grow from one point, because the thickness of the NBs depends on the gold diameter. Therefore, two nanorings with different diameters grow from one point and form dual-nanorings. Addition of these mechanism, it can be described the extent of Sn doping into ZnO and its role in the formation of nanorings. In fact, if the planar defects are formed due to existence of the Sn in the ZnO structure, then Sn should have a critical concentration in ZnO.[25] Therefore, ZnO nanorings cannot be formed in lower Sn concentration level due to not formed planar defects. In fact, the nanorings have been formed after a critical dopant of Sn in the ZnO structures. Therefore, we could observe ZnO nanorings in the sample, which were grown at 700 ºC, with high concentration of Sn clearly, while, another Sn-doped ZnO NBs with lower Sn concentration shows different shape of nanorings (Fig. 1(e).

Figure 4 (a-c) shows high resolution N (E) Auger electron spectroscopy (AES) of tin, oxygen, and zinc, respectively for the Sn-doped ZnO NBs. The AES spectra of tin (Fig. 4 (a)) indicate clear peaks at 420 and 424eV for the both samples that corresponding to the MNN Auger electron emission from tin. Figure 3 (b) shows spectra of oxygen that indicate peaks at 484 and 504eV for the both samples that corresponding to the KLL Auger electron emission of oxygen. In addition, Fig. 3 (c) shows spectra of zinc that indicate peaks at 820, 895, 900, 911, 983 and 1006eV that corresponding to the LMM Auger electron emission of zinc. According to the peak areas of the Sn, the Sn concentration of the sample grown at 800 ºC is lower than other sample that is good agreement with the EDX results. In addition, the Sn concentration was compared between two places of the NBs, one at the centre of the NBs and other at the edge of the NBs. It was observed that, the Sn concentration is higher at the centre in comparison to the edge of the NBs.

Figure 5 shows the XRD patterns of the undoped and Sn-doped ZnO NBs. The XRD patterns in Fig. 5 agreed with the standard card of bulk ZnO with hexagonal structure (JCPDS No. 800075) and no diffraction peaks of other impurity such as SnO and SnO_2 were detected. However, due to sensitivity limitation of the XRD device such peaks cannot be seen.

Optical properties of the samples were studied by two methods to obtain band gap of the samples and to investigate optical applications of the samples. The DRS measurements now have been used to measure the optical absorption properties of the NBs that could not be recorded in the transmission mode.[26-27] In this case, the UV-vis DRS of the undoped and Sn-doped ZnO NBs are shown in Fig. 6 (a). It can be seen an obvious blue-shift in absorption edge for the Sn-doped ZnO NBs in comparison to the undoped ZnO NBs that is good agreement with the PL results. Moreover, the direct band gap energies estimated from a plot of $(\alpha\times h\nu)^2$ versus the photo energy ($h\nu$) according to the Kubelka-Munk model,[28] as shown in the inset of Fig 6 (a) are 3.27, 3.37, and 3.46 eV for the undoped ZnO NBs, Sn-doped ZnO NBs grown at 800 ºC, and Sn-doped ZnO NBs grown at 700 ºC. Figure 6 (b) shows the room temperature PL spectra of the ZnO nanobelts. There are two bands in the PL spectra of the products, one of them related to the ultraviolet (UV) emission at 375-383nm (3.25-3.30eV) and the other related to the deep level emission (DLE) at 513-526nm (2.36-2.42eV). The UV emission is also called the near band edge (NBE) emission, due to the recombination of free excitons through an exciton-exciton collision process. It has been suggested that the green band emission corresponds to the singly ionized oxygen vacancy in ZnO and results from the recombination of a photo-generated hole with the singly ionized charge state of this defect. Thus, the weak green band of the undoped ZnO NBs in the PL spectrum shows that there are very low concentrations of oxygen

vacancies. The PL spectra also show a blue shift for UV peaks of the Sn-doped ZnO NBs in comparison to the UV peak of the undoped ZnO NBs. In addition, these spectra reveal that, crystalline quality of the undoped ZnO NBs is higher than the crystalline quality of the Sn-doped ZnO NBs. Therefore, the both optical characterizations show that, the Sn-doped ZnO NBs have capability to fabricate UV detectors and sources in the future.

For more understanding of the obtained PL spectra, the undoped and Sn-doped ZnO NBs, which were grown at 700 ºC, were characterized by XPS analysis. Figure 7 (a) and (b) show the XPS spectra of Zn 2p of undoped and Sn-doped ZnO NBs, respectively. It can be seen, the spin–orbit splitting of 23 eV for Zn-$2p_{3/2}$ and Zn-$2p_{1/2}$ confirms that the Zn atoms are in a completely oxidized state for both samples. The Sn-3d binding energies region consists of an asymmetric peak that could be fitted with two doublets assigned tentatively to the Sn-$3d_{5/2}$ and $3d_{3/2}$ core levels (Fig. 7 (c)). The splitting of 8.4 eV for Sn-$3d_{5/2}$ and Sn-$3d_{3/2}$ indicates that the Sn atoms are in the SnO_2 state.[29] The O 1s spectra of undoped and Sn-doped ZnO NBs are shown in Figs. 7 (d) and (e), respectively. In the O 1s region, symmetric broad peak related to the low and higher binding energy components at around 531 eV and 533 eV, respectively. The 531 eV peak is attributed to the O^{2-} ions on the wurtzite structure of the hexagonal Zn^{2+} ion array, which are surrounded by zinc atoms with the full supplement of nearest-neighbour O^{2-} ions. Therefore, the 531 eV peak of the O1s spectrum can be attributed to the Zn–O bonds (O_L). Meanwhile, the higher binding energy component at 533 eV is assigned to the oxygen vacancies within the ZnO matrix (O_V).[30] Figures 7 (d) and (e) show that, the proportion of O_V in the non-lattice oxygen of Sn-doped ZnO NBs is higher than proportion of O_V in the non-lattice oxygen of undoped ZnO NBs. The changing trend of oxygen vacancy in the non-lattice oxygen agrees with the relative percentage of green emission from PL spectra of the undoped and Sn-doped ZnO NBs. It has been reported such relationship between XPS and PL results in other works of ZnO researches.[31-32]

Conclusions

Sn-doped ZnO dual-nanorings and NBs were grown with the assisted VLS approach using the thermal evaporation method. The HRTEM image and SAED pattern showed that the Sn-doped ZnO NBs grew along the $[01\bar{1}0]$ direction. In addition, these results indicated that using Sn as an impurity caused planar defects along the length of the NBs. It was observed that such planar defects played an important role in the creation of ZnO nanorings. Furthermore, the FESEM images and EDX spectra showed that nanorings with a dual shape were formed at the ends of the NBs that were grown using the VLS approach. Our observations determined that dual nanorings were formed as a result of the instability of the gold particle during the growth process. Finally, the optical properties of the Sn-doped and undoped ZnO NBs were studied, and it was observed that Sn could cause to widen band gap of ZnO nanostructures. Therefore, such optical properties can be a potential for ZnO NBs and nanorings as UV detectors or sources.

Acknowledgments

This work was supported through the Islamic Azad University (I.A.U), Masjed-Soleiman Branch. I acknowledge Dr. F. Jamali-Sheini from I.A.U, Ahwaz Branch for his useful comments about XPS results.

.Notes and references

Department of Physics, Islamic Azad University, Masjed-Soleiman Branch, Masjed-Soleiman, Iran. Fax: +986143260093; Tel: +989166224993; E-mail: Yousefi.ramin@gmail.com, yousefiramin@iaumis.ac.ir

1 B. Murali, J. Parui, M. Madhuri, S.B. Krupanidhi, *J. Phys. D: Appl. Phys.* 2015, **48,** 015301.
2 W-K. Hong, J.I. Sohn, D-K. Hwang, S-S Kwon, G. Jo, S. Song, S-M. Kim, H-J Ko, S-J Park, M.E. Welland, T. Lee, *Nano Lett*. 2008, **8**, 950.
3 Y. Ding, X.Y. Kong, Z.L. Wang, *Phys Rev B* 2004, **70,** 235408.
4 Z.L. Wang, *J. Phys.: Condens. Matter* 2004, **16,** R829.
5 Z.W. Pan, Z.R. Dai, Z.L. Wang, *Science* 2001, **291,** 1947.
6 W.L. Hughes and Z.L. Wang*, J. Am. Chem. Soc*. 2004, **126,** 6703.
7 X.Y. Kong, Y. Ding, R. Yang, Z.L. Wang, *Science* 2004, **303,** 1348.
8 E. Pa´l, V. Hornok, A. Oszkoo´, I. De´ka´ny, *Colloid Surface A.* 2009, **340**, 1.
9 M.N. Jung, S.H. Ha, S.J. Oh, J.E. Koo, Y.R. Cho, H.C. Lee, T.I. Jeon, H. Makino, J.H. Chang, *Curr Appl Phys* 2009, **9**, 169.
10 R. Yousefi, F. Jamali-Sheini, A. Khorsand Zak, M.R. Mahmoudian, *Ceram Int* 2012, **38**, 6295.
11 R. Yousefi, M.R. Muhamad, A. Khorsand Zak, *Thin Solid Films* 2010, **518**, 5971.
12 R. Deng, X. Zhang, E. Zhang, Y. Liang, Z. Liu, H.Y. Xu, S. Hark, *J. Phys. Chem. C,* 2007, ***111*,** 13013.
13 Y. Ding, P.X. Gao, Z.L. Wang, *J. Am. Chem. Soc.*, 2004, **126,** 2066.
14 J. Zhao, C. Ye, X. Fang, L. Qin, L. Zhang, *Cryst. Growth & Des* 2006, **6,** 2643.
15 R. Deng, X.T. Zhang, *J. Luminescence* 2008, **128,** 1442.
16 L. Shi, Y. Xu, S. Hark, Y. Liu, S. Wang, L.M. Peng, K. Wong, Q. Li, *Nano Lett* 2007, **7**, 3559.
17 S.Y. Li, P. Lin, C.Y. Lee, T.Y. Tseng, C.J. Huang, *J. Phys. D: Appl. Phys.* 2004, **37,** 2274.
18 Q. Kuang, Z.Y. Jiang, Z.X. Xie, S.C. Lin, Z.W. Lin, S.Y. Xie, R.B. Huang, L.S. Zheng*, J. Am. Chem. Soc* 2005, **127,** 11777.
19 F. Jamali-Sheini, M.A. More, S.R. Jadkar, K.R. Patil, V.K. Pillai, D.S. Joag, *J. Phys. Chem. C* 2010, **114**, 3843.
20 S.Y. Li, P. Lin, C.Y. Lee, T.Y. Tseng, C.J. Huang*, J. Phys. D: Appl. Phys.* 2004, **37,** 2274.
21 R. Deng, X. Zhang, E. Zhang, Y. Liang, Z. Liu, H.Y. Xu, S. Hark*, J. Phys. Chem. C* 2007, **111,** 13013.
22 R. Yousefi, F. Jamali-Sheini, A. Khorsand Zak, *Chem. Vapor. Depo* 2012, **18,** 215.
23 X.Y. Kong and Z.L. Wang, *Nano Lett*. 2003, **3,** 1625.
24 N. Wang, Y. Cai, R.Q. Zhang, *Mat Sci Eng R* 2008, **60**, 1.
25 Y.C. Park, Y.H. Kim, H-H. Nahm, J-Y. Noh, Y-S Kim, J. Kim, W.S. Lee, J-M Yang, J. Park, Appl. Phys. Lett. 2013, **102**, 033103.
26 L. Wang, H. Li, S. Xu, Q. Yue, J. Liu, *Mater Chem Phys*, 2014, **147,** 1134.
27 F. Jamali-Sheini and R. Yousefi, *Ceram Int* 2013, **39,** 3715.
28 A. Khorsand Zak, R. Yousefi, F. Jamali-Sheini, M.R. Muhamad, *Ceram Int* 2012, **38,** 2059.
29 J.G. Kim, S.H. Lee, S.H. Nam, S.M. Choi, W.B. Kim, *RSC Adv.*, 2012,**2**, 7829.

30 J.H. Zheng, Q. Jiang, J.S. Lian, *Appl Surf Sci* 2011, **257** 5083.
31 X-G. Han, H-Z He, Q. Kuang, X. Zhou, X-H Zhang, T Xu, Z-X. Xie, L-S. Zheng, *J. Phys. Chem. C* 2009, **113**, 584–589.
32 H. Tian, J. Xu, Y. Tian, P. Deng, H. Wen, *CrystEngComm*, 2013, **15**, 5345.

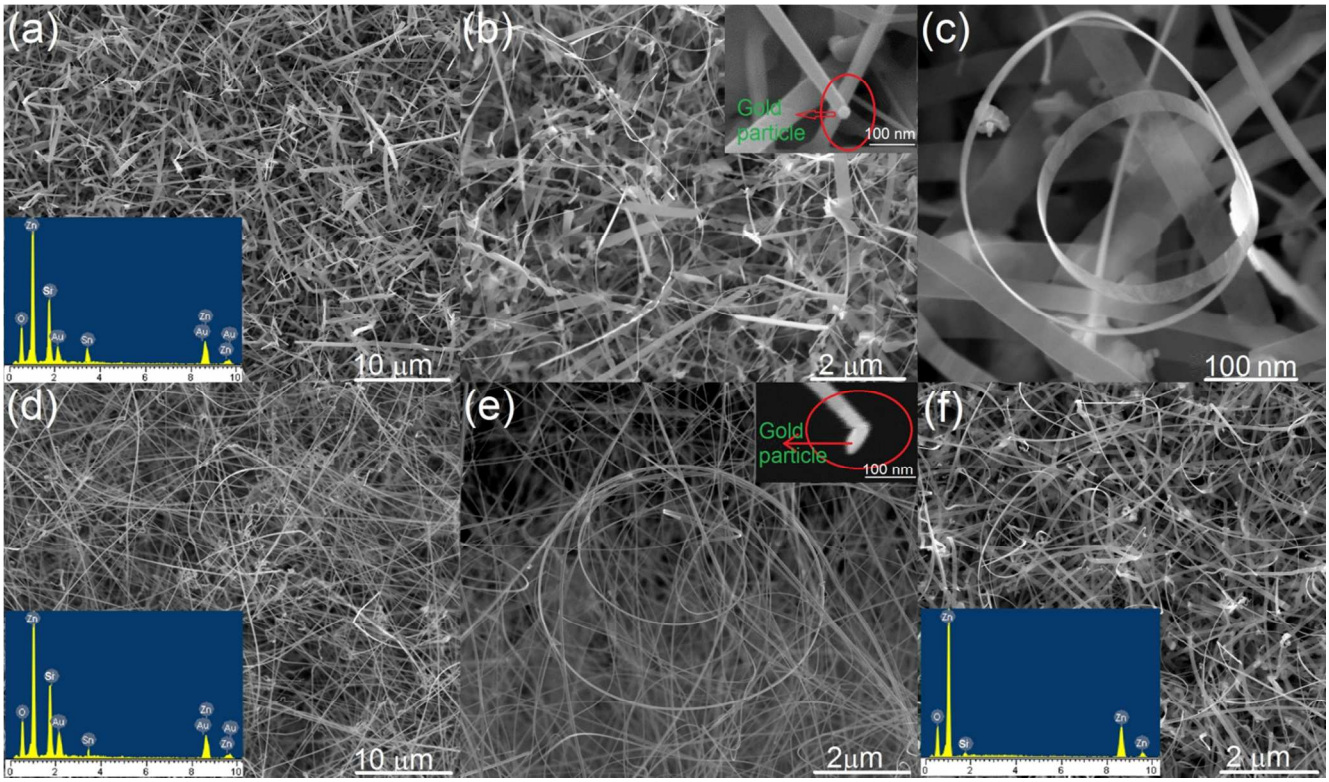

Figure 1. (a) and (b) Low and high magnification FESEM images of Sn-doped ZnO NBs that were grown on Si substrate at 700 °C. EDX spectrum of these NBs is shown in Fig. (a). The inset of Fig (b) shows a single nanobelt that was grown with a gold particle at on its tip. (c) Shows a dual Sn-doped nanoring that is formed at 700 °C. (d) and (e) Low and high magnification FESEM images of Sn-doped ZnO NBs that were grown on Si substrate at 800 °C. EDX spectrum of these NBs is shown in Fig. (d). The inset of Fig (e) shows a single nanobelt that were grown with a gold particle at on its tip. FESEM image and EDX spectrum of undoped ZnO NBs.

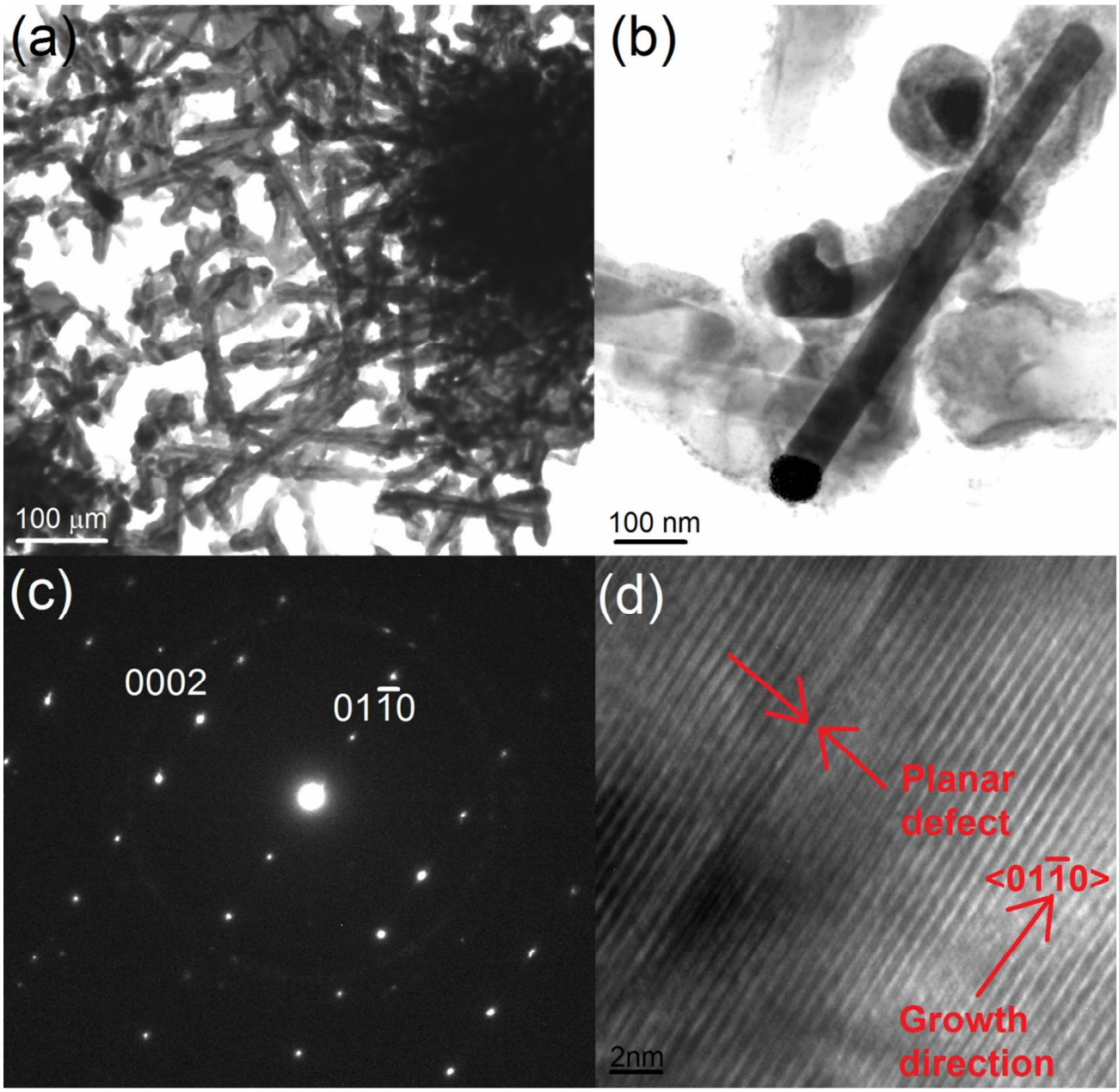

Figure 2. (a) TEM image of Sn-doped ZnO NBs that were grown at 700 °C. (b) TEM image of a single Sn-doped ZnO nanobelt with gold particle that were created on the tip of the nanobelt. (c) SAED pattern of a single Sn-doped ZnO nanobelt. (d) HRTEM image of a single Sn-doped ZnO nanobelt. Planar defect line due to existence of Sn is indicated by arrows.

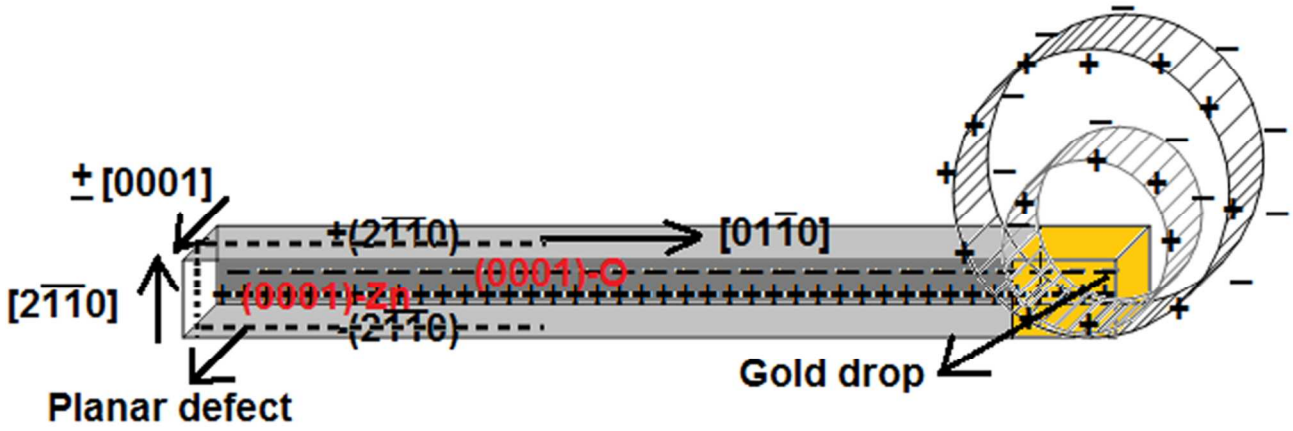

Figure 3. Schematic of a single nanobelt and a dual nanoring that was attached to the nanobelt. It can be seen that, the nanobelt grown along [01$\bar{1}$0] direction with up and down ±(2$\bar{1}\bar{1}$0) surfaces and side ±(0001) surfaces. In addition, planar defect that was formed parallel with [01$\bar{1}$0] direction and plane of this defect parallel with ±(0001) surfaces. Yellow part shows gold particle.

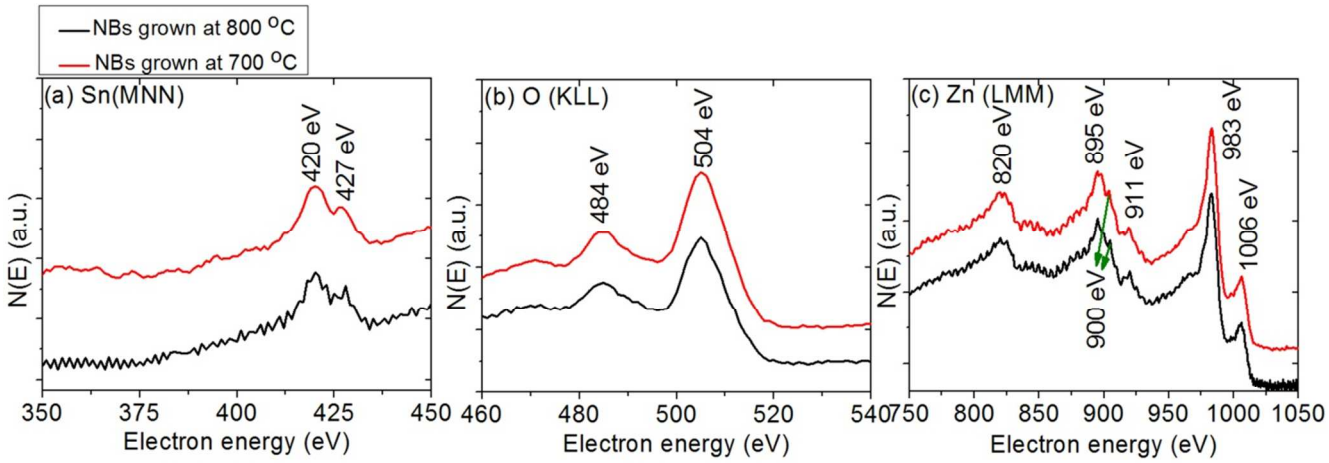

Figure 4. High resolution N (E) Auger electron emission spectroscopy of the ZnO nanobelts deposited on the Si substrates at 700 and 800 °C. (a) Sn-MNN spectra, (b) O-KLL spectra and (c) Zn-LMM spectra.

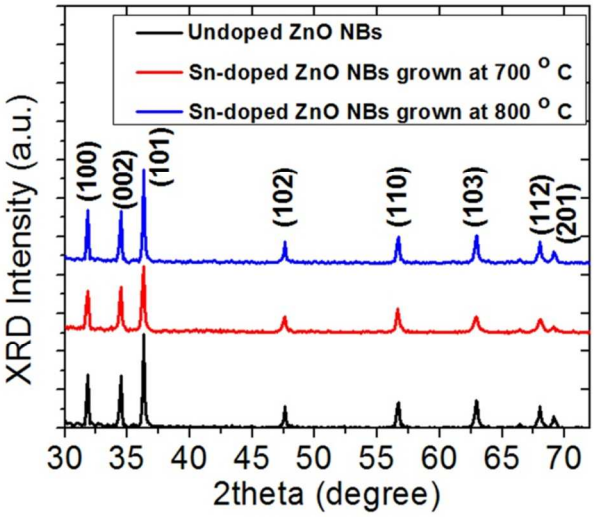

Figure 5. XRD patterns of undoped and Sn-doped ZnO NBs.

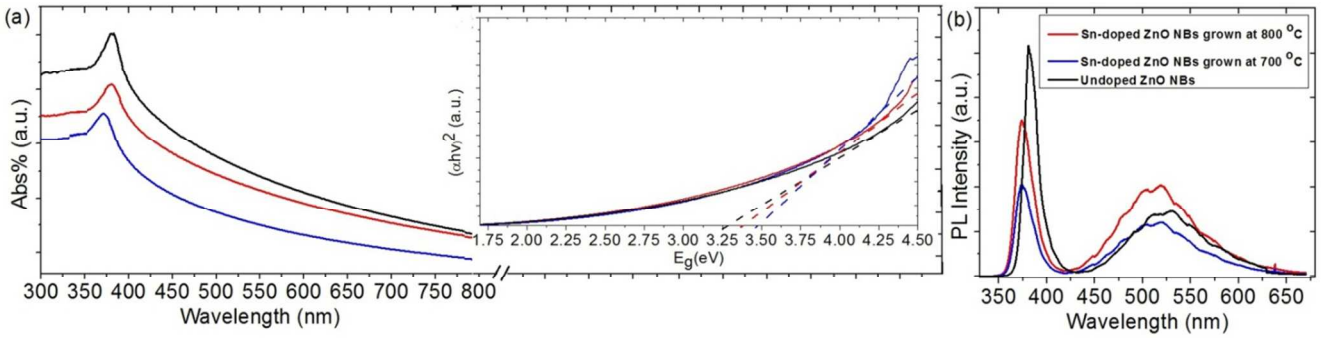

Figure 6. (a) DRS spectra of the undoped and Sn-doped ZnO NBs deposited at 700 and 800 °C. The inset shows estimating of band gap of the undoped and Sn-doped ZnO NBs using Kubelka–Munk method. (b) PL spectra of the undoped and Sn-doped ZnO NBs deposited at 700 and 800 °C.

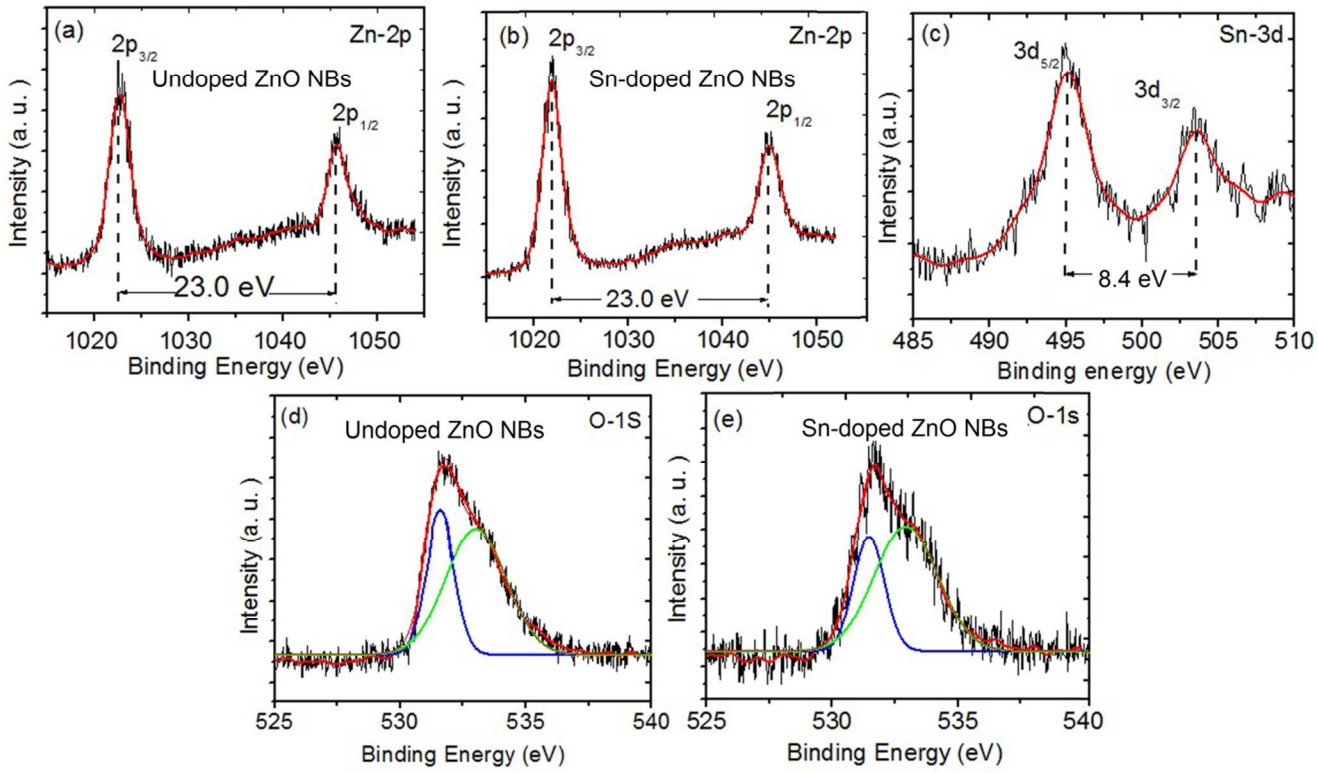

Figure 7. XPS spectrum of (a) Zn 2p of undoped ZnO NBs, (b) Zn 2p of Sn-doped ZnO NBs grown at 700 ºC, and (c) Sn 3d of Sn-doped ZnO NBs grown at 700 ºC. XPS spectrum of (d) O 1s of undoped ZnO NBs and (e) O 1s of Sn-doped ZnO NBs grown at 700 ºC.

ZnO dual-nanorings were formed due to create planar defects in nanobelts that were generated due to appearance of Sn atoms.